Monthly Notices
of the
ROYAL ASTRONOMICAL SOCIETY

Mon. Not. R. Astron. Soc. **414,** 2087–2100 (2011) doi:10.1111/j.1365-2966.2011.18522.x

Polarization observations of 20 millisecond pulsars

W. M. Yan,[1,2★] R. N. Manchester,[3] W. van Straten,[4] J. E. Reynolds,[3] G. Hobbs,[3] N. Wang,[1] M. Bailes,[4] N. D. R. Bhat,[4] S. Burke-Spolaor,[3,4] D. J. Champion,[3,5] W. A. Coles,[6] A. W. Hotan,[4,7] J. Khoo,[3] S. Oslowski,[3,4] J. M. Sarkissian,[3] J. P. W. Verbiest[4,5] and D. R. B. Yardley[3,8]

[1]*Urumqi Observatory, NAOC, 40-5 South Beijing Road, Urumqi, Xinjiang 830011, China*
[2]*Graduate University of Chinese Academy of Sciences, 19A Yuquan Road, Beijing 100049, China*
[3]*CSIRO Astronomy and Space Science, Australia Telescope National Facility, PO Box 76, Epping, NSW 1710, Australia*
[4]*Centre for Astrophysics and Supercomputing, Swinburne University of Technology, PO Box 218, Hawthorn, VIC 3122, Australia*
[5]*Max-Planck-Institut für Radioastronomie, Auf dem Hügel 69, 53121 Bonn, Germany*
[6]*Electrical and Computer Engineering, University of California at San Diego, La Jolla, CA 92093, USA*
[7]*Curtin Institute of Radio Astronomy, Curtin University, Bentley, WA 6102, Australia*
[8]*Sydney Institute for Astronomy, School of Physics, The University of Sydney, NSW 2006, Australia*

Accepted 2011 February 9. Received 2011 February 8; in original form 2010 November 24

ABSTRACT

Polarization profiles are presented for 20 millisecond pulsars that are being observed as part of the Parkes Pulsar Timing Array project. The observations used the Parkes multibeam receiver with a central frequency of 1369 MHz and the Parkes digital filter bank pulsar signal-processing system PDFB2. Because of the large total observing time, the summed polarization profiles have very high signal-to-noise ratios and show many previously undetected profile features. 13 of the 20 pulsars show emission over more than half of the pulse period. Polarization variations across the profiles are complex, and the observed position angle variations are generally not in accord with the rotating vector model for pulsar polarization. Nevertheless, the polarization properties are broadly similar to those of normal (non-millisecond) pulsars, suggesting that the basic radio emission mechanism is the same in both classes of pulsar. The results support the idea that radio emission from millisecond pulsars originates high in the pulsar magnetosphere, probably close to the emission regions for high-energy X-ray and gamma-ray emission. Rotation measures were obtained for all 20 pulsars, eight of which had no previously published measurements.

Key words: polarization – pulsars: general – radio continuum: stars.

1 INTRODUCTION

Soon after the discovery of pulsars, it was shown that the radio emission from pulsars is highly polarized (Lyne & Smith 1968). The mean pulse profile and polarization properties of a pulsar are important for understanding the pulse emission mechanism, the beaming of pulsar radiation and the geometry of the system. Mean pulse profiles often have a double or triple form, leading to a description of the emission in terms of 'core' and 'conal' beams (Backer 1976). Rankin (1983) suggested that the core and conal components had different emission mechanisms, whereas Lyne & Manchester (1988) argued that there was a gradual change in emission characteristics from the core region to the outer edge of the emission beam rather than distinct emission processes. To explain more complex pulse profiles, multiple emission cones were proposed and discussed by several authors (Rankin 1993; Kramer 1994; Gupta & Gangadhara 2003). An alternative model suggests that the emission beam of a pulsar is filled with randomly distributed emission patches (Lyne & Manchester 1988; Manchester 1995; Han & Manchester 2001). The patchy model may explain more complicated multicomponent and asymmetric pulse profiles.

Polarization properties of radio sources are normally described in terms of the Stokes parameters: I (total intensity), Q and U (linear polarization) and V (circular polarization). Many pulsars show a systematic variation of the position angle (PA), ψ, of the linearly polarized emission,

$$\psi = 0.5 \tan^{-1}(U/Q), \quad (1)$$

across the pulse profile. In many pulsars, the observed PA variations can be approximately described by the 'rotating vector model' (RVM, Radhakrishnan & Cooke 1969). This model originates from the idea that the radiation is polarized in the plane of curvature of field lines emanating from a magnetic pole on the star; not

★E-mail: yanwm@uao.ac.cn

surprisingly, curvature radiation has this property (Komesaroff 1970). For a simple dipole field, the observed PA variation is then determined by the projected direction of the magnetic axis as the star rotates. The rapid swings often observed near the profile mid-point imply that magnetic axis is nearly aligned with the observer's line of sight at that profile phase. Circular polarization (Stokes V) is usually relatively weaker than linear polarization. It is most often associated with the central or core component of the profile, often with a sense reversal near the profile mid-point (Rankin 1983). Observed PA swings are not always smooth and continuous. Discontinuities of approximately 90° are often observed (e.g. Manchester, Taylor & Huguenin 1975; Backer & Rankin 1980; Stinebring et al. 1984; Han et al. 2009), and these are interpreted as resulting from overlapping emission from orthogonally polarized emission modes (e.g. McKinnon & Stinebring 1998). Such orthogonal modes may be generated as the wave propagates through the pulsar magnetosphere (e.g. Petrova 2001).

In many respects, millisecond pulsars (MSPs) have very different properties to those of 'normal' pulsars. Besides their obviously shorter periods, they have much smaller period derivatives and hence larger characteristic ages and weaker implied dipole magnetic fields. The pulse profile for MSPs generally has a much larger duty cycle, i.e. the emission covers a much larger fraction of the pulse period, and a more complicated pulse profile compared to normal pulsars (see e.g. Navarro et al. 1997; Kramer et al. 1998). This might be expected within the context of the magnetic pole model since the pulsar magnetosphere, bounded by the light cylinder of radius $R_{\rm LC} = cP/2\pi$ is so much smaller. Consequently, the polar caps defined by the open field lines (those that penetrate the light cylinder) are larger and the opening angle of these open field lines at a given radial distance r and fractional polar cap radius s is also larger:

$$\theta_b \approx \frac{3}{2} s \left(\frac{r}{R_{\rm LC}} \right)^{1/2} \tag{2}$$

where θ_b is the field-line tangent angle with respect to the magnetic axis (see e.g. Dyks, Wright & Demorest 2010b). Despite these differences, the polarization characteristics of MSPs are remarkably similar to those of normal pulsars – they have similar high degrees of linear polarization, orthogonal mode PA jumps are observed and circular polarization with sense changes near the profile centre is seen in some MSPs (see e.g. Thorsett & Stinebring 1990; Navarro et al. 1997; Stairs, Thorsett & Camilo 1999; Manchester & Han 2004; Ord et al. 2004). Although the emission characteristics are similar, indicating that the emission mechanism is basically the same for normal pulsars and MSPs, the PA variations in MSPs are often more complex and do not fit the RVM well.

Faraday rotation occurring in the interstellar medium is relatively easy to observe in pulsars because of the typically high degree of linear polarization. Faraday rotation is quantified by the rotation measure (RM), defined by

$$\psi = {\rm RM}\, \lambda^2, \tag{3}$$

where $\lambda = c/\nu$ is the radio wavelength corresponding to radio frequency ν. Faraday rotation in the interstellar medium is given by

$${\rm RM} = 0.810 \int_0^D n_{\rm e} \boldsymbol{B} \cdot {\rm d}l, \tag{4}$$

where $\boldsymbol{B}$ is the vector magnetic field in microgauss and the integral is over the path to the pulsar, and so observations of Faraday rotation can be used to investigate the Galactic magnetic field (see e.g. Manchester 1974; Han et al. 2006; Noutsos et al. 2008). Pulsars have the unique advantage that the dispersion measure (DM),

$${\rm DM} = \int_0^D n_{\rm e}\, {\rm d}l, \tag{5}$$

is also known. We can therefore obtain a measure of the mean line-of-sight component of the interstellar magnetic field weighted by the local electron density along the path:

$$\langle B_{||} \rangle = 1.232\, \frac{\rm RM}{\rm DM}\, \mu{\rm G}, \tag{6}$$

where RM and DM are in their usual units.

In this paper, we report on the mean pulse profiles and polarization properties of the 20 MSPs which are being observed as part of the Parkes Pulsar Timing Array (PPTA) project (Manchester 2008; Hobbs et al. 2009). Details of the observing system and the observations are given in Section 2, and polarization profiles for the 20 pulsars are presented in Section 3. RM results are presented in Section 4, and the implications of the results are discussed in Section 5.

2 OBSERVATIONS AND ANALYSIS

As part of the PPTA project, frequent observations of 20 MSPs are made using the Parkes 64-m radio telescope. Regular observations at approximately three-weekly intervals commenced in mid-2004. Since that time, back-end signal processing systems have been upgraded several times. The main objective of these observations is to detect gravitational waves through high-precision pulsar timing. However, there are many secondary objectives, including studies of the pulse emission properties for pulsars in the observed sample. All PPTA data are recorded in full-polarization mode, not only enabling full profile calibration, but also making possible detailed studies of the pulse emission properties. This paper reports on polarization results from observations made with the centre beam of the Parkes 20-cm Multibeam receiver (Staveley-Smith et al. 1996) with the second-generation Parkes digital filter bank system PDFB2 between 2007 June and 2009 November. The fact that many observations are available for all 20 pulsars means that pulse profiles with very high signal-to-noise ratios (S/N) can be formed, leading to new information about the profile shapes and their polarization.

Feeds in the Parkes 20-cm Multibeam receiver have orthogonal linearly polarized probes with a calibration probe at 45° to the two signal probes through which a linearly polarized broad-band and pulsed calibration signal can be injected. The system equivalent flux density on cold sky is approximately 30 Jy. In common with the other Parkes digital filter bank systems, PDFB2 digitizes band-limited signals from each of the two orthogonal probes at the Nyquist rate with 8-bit sampling. It uses field-programmable gate array (FPGA) processors to implement a polyphase filter to provide frequency resolution and a synchronous averager to form mean pulse profiles. For the observations reported here, the total bandwidth was 256 MHz centred at 1369 MHz with 1024 channels across the band for most of the 20 pulsars. For all, except PSR J1857+0943, PSR J1939+2134 and PSR J2124−3358, each observation was of 64-min duration; for the exceptions, the observation times were 32 min. All data were recorded using the PSRFITS data format (Hotan, van Straten & Manchester 2004) with 1-min subintegrations and the full spectral resolution. To provide a calibration of the gain and phase of the receiver system, the pulsed calibration signal was recorded for 2 min prior to each pulsar observation. Signal amplitudes were placed on a flux density scale using observations of Hydra A, assumed to have a flux density of 43.1 Jy at

1400 MHz and a spectral index of −0.91. The 20-cm multibeam feeds have limited isolation between the orthogonal polarizations. This cross-coupling was measured using series of observations of PSR J0437−4715 covering a wide range of hour angles, allowing correction for the effects of this coupling (van Straten 2004).

Offline data processing made use of the PSRCHIVE pulsar data analysis system (Hotan et al. 2004). First, band edges (5 per cent on each side) and spurious data resulting from narrow-band and impulsive radio frequency interference (RFI) were effectively excised from the raw data files. Typically, 1–2 per cent of the spectrum and the time domain data were excised. The data were then averaged in time to give eight subintegrations for each observation. Next, the data for each observation were corrected for variations in instrumental gain and phase across the spectrum and for the effects of cross-coupling in the feed. Finally, baselines for each of the Stokes-parameter profiles were set to zero mean and the data placed on a flux density scale. The baseline region was computed from the Stokes I profile and applied to all four Stokes-parameter profiles. Following this calibration, Stokes parameters were in accordance with the astronomical conventions described by van Straten et al. (2010). Specifically, PAs are absolute and are measured from celestial north towards east, i.e. counterclockwise on the sky, and Stokes V is defined as $I_{\rm LH} - I_{\rm RH}$, using the IEEE definition for sense of circular polarization.

In order to form final mean polarization profiles, it is necessary to sum across the frequency channels taking into account the Faraday rotation across the band. Sufficiently precise RM measurements were not previously available for most of the PPTA sample. We therefore determined RM values for each pulsar from the PDFB2 data sets. For each individual observation, the upper and lower halves of the total band were separately summed using the nominal RM value. An improved value of the RM was then calculated by taking a weighted mean of PA differences for bins where the uncertainty in PA was less than 10°. This process was iterated until convergence was obtained. The contribution of the Earth's ionosphere to the total RM was estimated and then subtracted so that the measured RM just represents the interstellar contribution. Ionospheric RMs were computed using a prediction program FARROT, developed at the Dominion Radio Astrophysical Observatory, Penticton, which uses the observed solar 10.7-cm radio flux as a basic input. As the observations were made near a minimum of solar activity, ionospheric RMs are relatively small, typically between −0.5 and −1.0 rad m^{-2}. The final interstellar RM for each pulsar was determined by taking a weighted mean of the individual interstellar RM measurements. In addition, the observed Stokes parameters for each observation were adjusted (effectively a PA shift) using the ionospheric RM so that they represent the polarization state at the top of the ionosphere.

It is also necessary to have a precise timing model for each pulsar before adding the data in time to form a final mean profile. Pulse times of arrival were obtained for each observation using an analytic template based on an existing high S/N pulse profile. The TEMPO2 pulsar timing package (Hobbs, Edwards & Manchester 2006) was then used to fit pulsar spin and astrometric and binary parameters as necessary to give 'white' timing residuals for the PDFB2 data set for each pulsar. Finally, the separate observations were summed using this timing model to determine relative phases to form the final Stokes-parameter profiles. To give the best possible S/N in the final profile, the individual observation profiles were weighted by their $(\mathrm{S/N})^2$ when forming the sum profile. The polarization parameters $L = (Q^2 + U^2)^{1/2}$, $|V|$ and PA were then computed from the Stokes parameters. The noise bias in L was corrected using the relations given by Lorimer & Kramer (2005), and the similar bias in $|V|$ was corrected using

$$|V|_{\rm corr} = \left(|V|^4 - \sigma_I^4\right)^{1/4} \quad (7)$$

when $|V| > \sigma_I$ or zero otherwise, where σ_I is the rms profile baseline noise.

Table 1 gives the basic pulsar and observational parameters for the 20 PPTA pulsars which were observed. After the pulsar name, pulse period and DM, we give the number of frequency channels across the 256-MHz band and the number of bins across the pulse period. The dispersion smearing across each frequency channel, given by

$$\Delta t_{\rm DM} \approx 8.30 \times 10^6\ \mathrm{DM}\ \Delta f\ f^{-3}\ \mathrm{ms}, \quad (8)$$

where Δf is the channel width in MHz, f is the band centre frequency in MHz, and the DM is in units of cm^{-3} pc, is given in units of profile bins. The last two columns give the number of observations summed and the total observation times in the remaining three channels.

3 POLARIZATION PROFILES

Polarization profiles at 1369 MHz for the 20 PPTA MSPs are presented and discussed in this section. Table 2 gives a summary of the results. Columns (2) and (3) give the mean flux density $S = \langle I \rangle$ averaged over all observations and its uncertainty. The next column gives the rms fluctuation in individual-observation flux densities. For low DM pulsars (DM $\lesssim$ 30 cm^{-3} pc), the rms fluctuation is comparable to or even greater than the mean value. This entirely results from intensity modulations due to diffractive interstellar scintillation. Pulse widths at 50 per cent of the peak flux density (W50) and 10 per cent of the peak (W10) are given next, both in degrees of longitude, where 360° is equivalent to the pulse period or 1.0 in pulse phase, and in milliseconds. The next column gives the overall pulse width measured from the first point to the last point where the pulse intensity significantly exceeds the baseline noise (more than three times the baseline rms noise in several adjacent bins). The next column gives the minimum number of identifiable pulse components in the pulse profile. A component is identified by a peak or, for overlapping components a significant inflection, in the pulse profile. The next three columns give the fractional linear polarization $\langle L \rangle / S$, the fractional net circular polarization $\langle V \rangle / S$ and the fractional absolute circular polarization $\langle |V| \rangle / S$ averaged over all observations, where the $\langle\rangle$ means are taken across the pulse profile.

In the following subsections, we present polarization profiles and discuss each pulsar in turn.

3.1 PSR J0437−4715

Mean pulse profile and polarization parameters for this very strong southern MSP (mean flux density about 145 mJy, Table 2) at 1369 MHz are given in Fig. 1. Our results are in good agreement with and extend previously published results (Johnston et al. 1993; Manchester & Johnston 1995; Navarro et al. 1997). As is well known, the total intensity and polarization variations across the pulse profile are complex. There are multiple overlapping components, and the present results show that the pulse profile extends over at least 85 per cent of the pulse period. The notches in Stokes I and L discussed by Navarro et al. (1997) and Dyks, Rudak & Rankin (2007) are clearly visible in the central expanded plot. The observed PA variations cannot be described by the RVM, even if orthogonal mode jumps are taken into account. There is a clear orthogonal

Table 1. Observational parameters for the 20 PPTA MSPs.

PSR	P (ms)	DM ($\mathrm{cm^{-3}\,pc}$)	No. of channels	No. of bins	DM smear (bins)	No. of obs.	Integ. time (h)
J0437−4715	5.757	2.64	1024	1024	0.4	92	96.3
J0613−0200	3.062	38.78	1024	512	5.2	41	43.3
J0711−6830	5.491	18.41	1024	512	1.4	28	29.1
J1022+1001	16.453	10.25	1024	2048	1.0	34	34.3
J1024−0719	5.162	6.49	1024	1024	1.0	29	30.0
J1045−4509	7.474	58.17	2048	512	1.6	33	34.1
J1600−3053	3.598	52.33	1024	512	6.0	28	29.7
J1603−7202	14.842	38.05	1024	1024	2.1	23	23.7
J1643−1224	4.622	62.41	1024	512	2.8	34	36.1
J1713+0747	4.570	15.99	1024	1024	2.9	40	40.7
J1730−2304	8.123	9.62	1024	1024	1.0	23	23.7
J1732−5049	5.313	56.82	2048	512	2.2	24	24.7
J1744−1134	4.075	3.14	512	1024	1.3	33	34.4
J1824−2452	3.054	120.50	2048	256	4.1	27	28.0
J1857+0943	5.362	13.30	1024	1024	2.1	26	13.4
J1909−3744	2.947	10.39	1024	512	1.5	67	69.6
J1939+2134	1.558	71.04	1024	256	9.4	26	13.8
J2124−3358	4.931	4.60	1024	1024	0.8	25	13.1
J2129−5721	3.726	31.85	1024	512	3.5	25	25.5
J2145−0750	16.052	9.00	1024	2048	0.9	29	29.6

Table 2. Flux density and polarization parameters for PPTA pulsars.

PSR	S	σ_S	S_{RMS}	W50		W10		Overall width	No. of	$\langle L\rangle/S$	$\langle V\rangle/S$	$\langle\lvert V\rvert\rangle/S$
	(mJy)	(mJy)	(mJy)	(°)	(ms)	(°)	(ms)	(°)	comp.	(per cent)	(per cent)	(per cent)
J0437−4715	149.3	4.0	38.0	9	0.14	64	1.02	306	12	24	−5	11
J0613−0200	2.3	0.1	0.6	55	0.92	108	8.18	158	7	15	2	4
J0711−6830	1.4	0.3	2.0	124	1.90	169	2.57	277	10	4	−3	4
J1022+1001	1.5	0.3	2.0	21	0.98	43	1.96	68	6	51	−11	14
J1024−0719	1.5	0.3	1.7	35	0.50	106	1.51	158	9	55	2	7
J1045−4509	2.2	0.1	0.5	37	0.76	70	1.45	248	9	20	13	14
J1600−3053	2.4	0.1	0.4	9	0.09	41	0.42	68	3	27	2	3
J1603−7202	4.2	0.7	3.4	29	1.21	41	1.71	238	7	17	27	28
J1643−1224	5.0	0.7	4.2	25	0.32	72	0.93	241	5	11	−1	9
J1713+0747	7.4	1.1	7.4	9	0.11	30	0.39	104	5	28	0	3
J1730−2304	3.9	0.3	1.5	43	0.98	77	1.74	232	9	27	−20	20
J1732−5049	1.3	0.1	0.5	20	0.29	119	1.76	155	4	7	0	2
J1744−1134	3.3	0.6	3.5	12	0.14	22	0.25	209	8	87	1	3
J1824−2452	1.6	0.1	0.6	115	0.98	189	1.60	281	6	58	1	6
J1857+0943	5.9	0.8	4.1	35	0.52	203	3.03	238	6	4	2	2
J1909−3744	2.6	0.2	2.0	5	0.04	11	0.09	187	3	47	12	13
J1939+2134	13.8	0.9	4.6	15	0.06	198	0.86	302	6	27	1	2
J2124−3358	2.4	0.4	2.1	38	0.53	275	3.76	331	12	18	0	3
J2129−5721	1.6	0.1	0.7	26	0.27	60	0.62	144	5	41	−23	26
J2145−0750	9.3	1.5	7.9	8	0.34	94	4.17	187	7	10	6	6

mode transition in both linear and circular polarization very close to the main profile peak and a non-orthogonal PA transition around pulse phase −0.23 (Manchester & Johnston 1995; Navarro et al. 1997). We also observe a probable non-orthogonal transition near pulse phase 0.35.

3.2 PSR J0613−0200

Fig. 2 shows the polarization profiles for PSR J0613−0200. These are consistent with and extend the 1341-MHz results presented by Ord et al. (2004). Stairs et al. (1999) observed very different profiles at 410 and 610 MHz,[1] indicating that there is significant profile morphology evolution between these lower frequencies and the 1369-MHz profile presented here. In particular, the trailing peak is much stronger at low frequencies relative to the rest of the profile. Our results have higher S/N than those previously published and

[1] Note that Stairs et al. (1999) uses a reversed PA sign compared to the International Astronomical Union (IAU) convention used here.

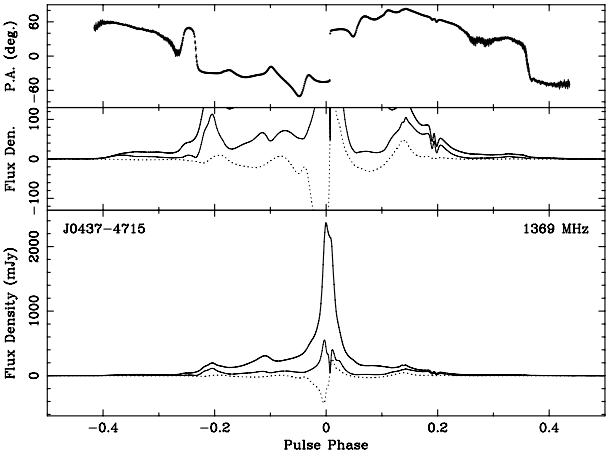

Figure 1. Polarization profiles for PSR J0437−4715 at 1369 MHz. The lower part gives the pulse profile for total intensity I (thick solid line), linearly polarized intensity L (thin solid line) and circularly polarized intensity V (dotted line). The middle part is an expanded plot showing low-level details of the polarization profiles, and the upper part gives the PA of the linearly polarized emission.

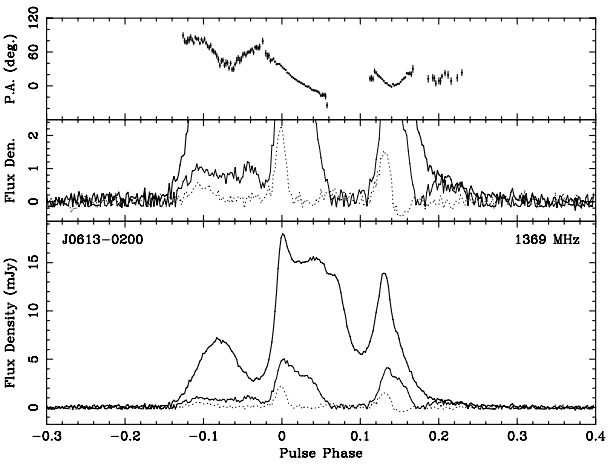

Figure 2. Polarization profiles for PSR J0613−0200 at 1369 MHz. See Fig. 1 for further details.

show that the pulse profile consists of multiple overlapping components; a weak trailing component was not obvious in previous results. Significant linear polarization is seen across essentially the whole profile, showing that the PA variations are more complex than was evident from earlier work, with several regions of increasing and decreasing PA across the profile. There is evidently a weak pulse component at the leading edge of the trailing component (at phase 0.12) which has a distinctly different PA, discontinuous with the rest of the trailing component. Two clear peaks in circular polarization are seen, under the leading edges of the central broad pulse peak and the trailing peak. There is a sense reversal in the circular polarization within the trailing component.

3.3 PSR J0711−6830

The mean pulse profile for this pulsar is basically a wide double with a connecting bridge of emission (Manchester & Han 2004; Ord et al. 2004). However, the results of Ord et al. (2004) showed that there were several overlapping components in the main peaks of the profile and furthermore that there was evidence for weak emission

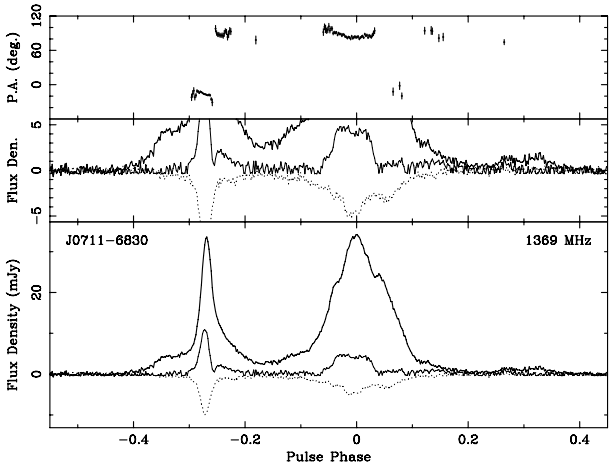

Figure 3. Polarization profiles for PSR J0711−6830 at 1369 MHz. See Fig. 1 for further details.

following the second main component, with significant emission over 75 per cent of the pulse period. These features are confirmed by the observations shown in Fig. 3. As well as the component preceding the first peak, there is clear emission following the second peak, with a low double-peaked feature close to phase 0.3 in Fig. 3. The polarization properties from our observations are very similar to those of Ord et al. (2004) with both linear and circular peaks centred under the main components. However, we find evidence for an orthogonal mode transition just after the peak of the leading main component.

3.4 PSR J1022+1001

Mean pulse profile and polarization parameters for this pulsar at 1369 MHz are given in Fig. 4. The polarization profiles shown here are generally in good agreement with those presented by Kramer et al. (1999), Stairs et al. (1999) and Ord et al. (2004), except that the fractional linear polarization in the trailing component in our observations is a little higher. Given that the overall PA variation closely fits the RVM, it seems probable that the PA glitch near the centre of the profile results from a separate emission component. Similar central PA discontinuities are seen in several pulsars, e.g. PSR B1913+16 (Blaskiewicz, Cordes & Wasserman 1991) and PSR J1141−6545 (Manchester et al. 2010). Alternatively, it may

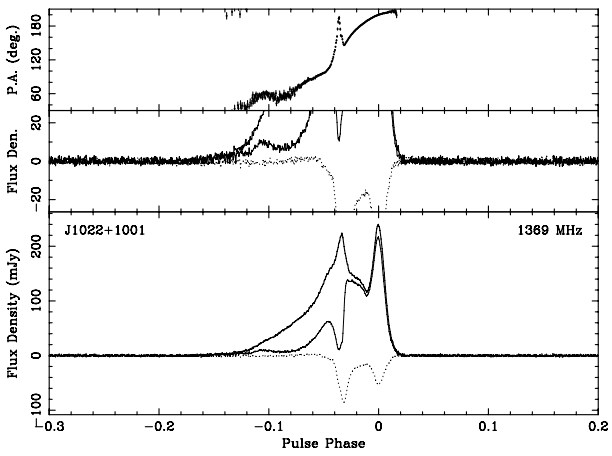

Figure 4. Polarization profiles for PSR J1022+1001 at 1369 MHz. See Fig. 1 for further details.

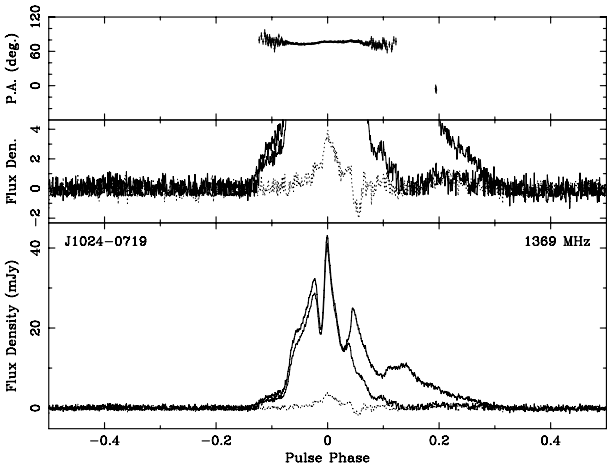

Figure 5. Polarization profiles for PSR J1024−0719 at 1369 MHz. See Fig. 1 for further details.

result from a pair of closely spaced and smeared orthogonal mode transitions.

3.5 PSR J1024−0719

Our results, presented in Fig. 5, have a higher S/N compared to earlier work (e.g. Ord et al. 2004) and show that the pulse profile has multiple overlapping features. The leading part of the profile has extremely high fractional linear polarization, whereas the trailing part of the profile is essentially unpolarized. Circular polarization is weak except near the centre of the profile where there is a sense reversal. There is a substructure in the circular polarization with at least three overlapping components in the positive V part. In agreement with previous work, we find that there is little or no variation in the PA across the profile.

3.6 PSR J1045−4509

Relatively low-quality polarization profiles have been presented for this pulsar by Ord et al. (2004) and Manchester & Han (2004). The data shown in Fig. 6 have higher S/N and show a number of previously unrecognized profile features. Most notable is the leading emission around phase −0.5 which is joined to the main pulse by a

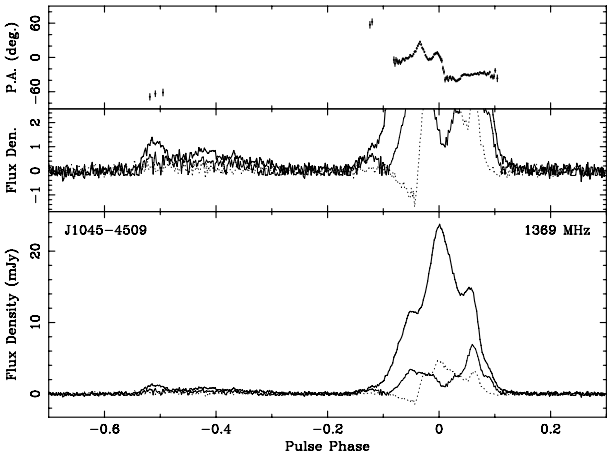

Figure 6. Polarization profiles for PSR J1045−4509 at 1369 MHz. See Fig. 1 for further details.

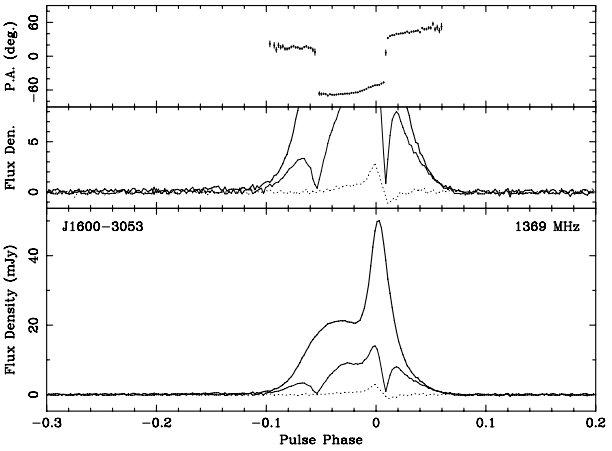

Figure 7. Polarization profiles for PSR J1600−3053 at 1369 MHz. See Fig. 1 for further details.

low-level bridge of emission. This low-level emission extends the overall pulse width to more than 60 per cent of the pulse period. The polarization properties shown in Fig. 6 are consistent with those given in the earlier papers but show more detail. In particular, the PA variation is more complex with non-monotonic variations and a probable orthogonal transition near the leading edge of the main pulse. There is a circular sense reversal between the first and second strong components of the main pulse.

3.7 PSR J1600−3053

Mean pulse profile and polarization parameters for this pulsar at 1369 MHz are shown in Fig. 7. Our observations are in complete agreement with those of Ord et al. (2004). Two orthogonal PA transitions are seen. The second of these slightly trails the strongest profile peak and is coincident with a sense reversal in V. This situation is virtually identical to that seen in PSR J0437−4715, with a fully orthogonal polarization transition very close to the main pulse peak.

3.8 PSR J1603−7202

Mean pulse profile and polarization parameters presented in Fig. 8 show that the profile for this pulsar has two main components,

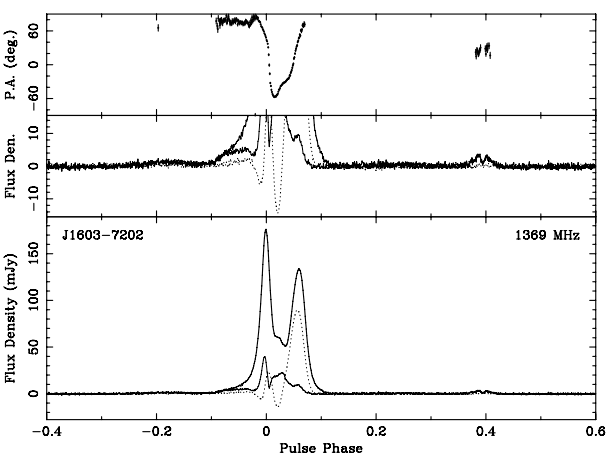

Figure 8. Polarization profiles for PSR J1603−7202 at 1369 MHz. See Fig. 1 for further details.

with the trailing one having very high circular polarization (cf. Manchester & Han 2004; Ord et al. 2004). Table 2 shows that this pulsar has the highest fractional mean V and $|V|$ of the PPTA pulsars. The expanded central plot in Fig. 8 shows that there is a broad low-level feature preceding the main pulse and a double-peaked pulse trailing the main pulse by about 0.4 in phase. With these additional pulse components, the pulse profile extends over about 70 per cent of the period. Variations in polarization across the pulse are complex with three sense reversals in V and an unusual PA variation which bears no relation to that expected for RVM.

3.9 PSR J1643−1224

The pulse polarization profiles given in Fig. 9 have far more details than previously published results (Stairs et al. 1999; Manchester & Han 2004; Ord et al. 2004). They show that the pulse profile has a long leading ramp (phase −0.6 to −0.3 in Fig. 9) followed by a broad component leading into the main pulse which has at least three overlapping components. There are two orthogonal polarization transitions near the pulse peak, and these are associated with sense reversals in V and dips in L. When account is taken of the two discontinuities, there is a decreasing PA through the stronger part of the profile, but with a significantly steeper PA swing in the trailing part. The PA of the broad feature preceding the main pulse is not very well determined, but it appears discontinuous with the rest of the PA variations.

3.10 PSR J1713+0747

Fig. 10 shows that this pulsar has a multicomponent mean pulse profile extending over a little more than 0.25 in phase. Our results are consistent with, but improve on, those of Ord et al. (2004). Both the leading and trailing parts of the pulse profile have very high, almost complete, linear polarization. Similar to PSR J1643−1224, there are two orthogonal PA transitions near the pulse peak. The second one of these is clearly associated with a sense change in V and the first may be also. A third PA transition is observed preceding the trailing pulse component. However, this is clearly not orthogonal, with $\Delta\psi \sim 70^\circ$.

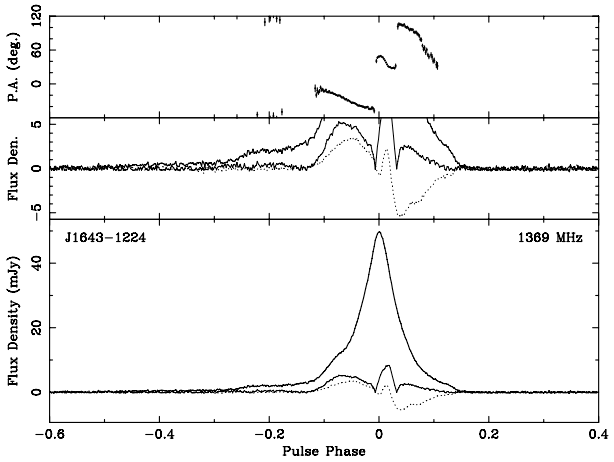

Figure 9. Polarization profiles for PSR J1643−1224 at 1369 MHz. See Fig. 1 for further details.

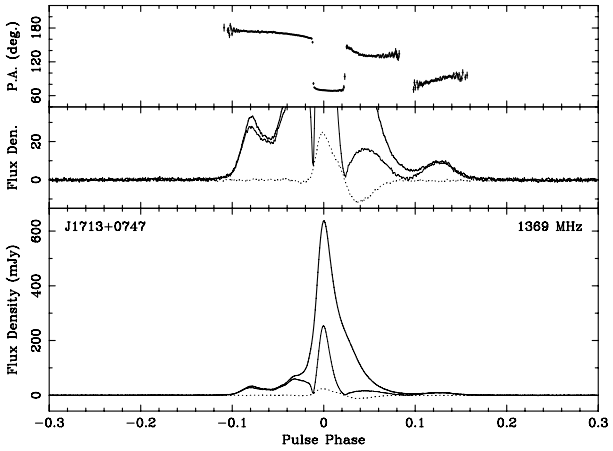

Figure 10. Polarization profiles for PSR J1713+0747 at 1369 MHz. See Fig. 1 for further details.

3.11 PSR J1730−2304

Mean pulse profile and polarization parameters for this pulsar at 1369 MHz are given in Fig. 11. These show that the pulse profile is very complex, with multiple components in the main part, two weak leading components (around phases −0.18 and −0.26) and a slightly stronger trailing component (around phase 0.32). The weak trailing component was also observed by Kramer et al. (1998), but the leading components have not been previously identified. This pulsar is unusual in that it has relatively strong right-circular polarization through much of the main pulse (cf. Ord et al. 2004). The observed PA variation is very complex with a possible orthogonal transition in the leading part of the main pulse. The rest of the profile shows complex PA variations with zones of both increasing and decreasing PA. Both the second precursor component and the post-cursor are highly linearly polarized, probably with increasing PA across them. The leading precursor is too weak to be sure about its polarization.

3.12 PSR J1732−5049

PSR J1732−5049 is a relatively weak pulsar. Results presented in Fig. 12 are similar to those given by Ord et al. (2004) except that the fractional linear polarization is a little higher. No significant circular polarization is observed across the profile. The PA swing is relatively flat with two PA jumps, both close to orthogonal.

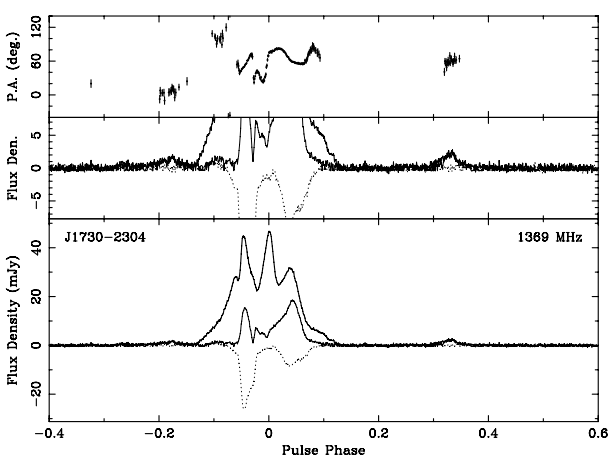

Figure 11. Polarization profiles for PSR J1730−2304 at 1369 MHz. See Fig. 1 for further details.

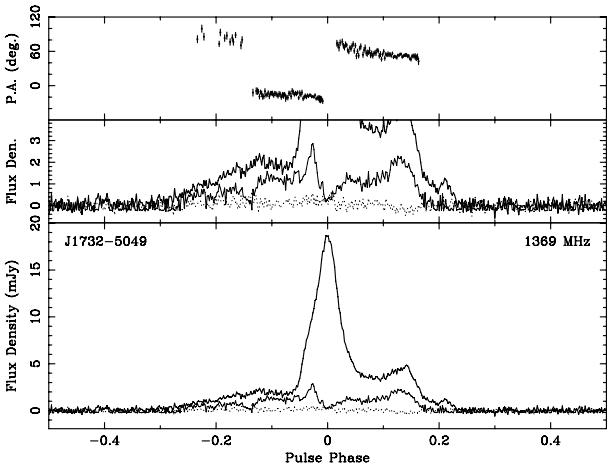

Figure 12. Polarization profiles for PSR J1732−5049 at 1369 MHz. See Fig. 1 for further details.

3.13 PSR J1744−1134

As shown in Fig. 13, the mean pulse profile of this pulsar has a sharp main pulse and a precursor preceding the main pulse by ∼0.35 in phase. The precursor was first detected by Kramer et al. (1998); these authors also found evidence for a post-cursor following the main pulse by about 0.2 in phase and amplitude about half of that of the precursor. We do not see this post-cursor component. Fig. 13 clearly shows that the precursor has multiple components. This pulsar is remarkable in that the main pulse is almost 100 per cent linearly polarized, especially on the leading edge. However, weak left-circular emission is observed in both the precursor and the main pulse. There is a smooth decrease of PA through the main pulse. This may be continuous with the PA of the precursor, indicating an outer line of sight, i.e. that the observer's line of sight is equatorwards of the magnetic axis.

3.14 PSR J1824−2452 (PSR B1821−24)

As Fig. 14 shows, this pulsar, which is located in the globular cluster M28 (Lyne et al. 1987), has a complex profile with multiple components covering more than 80 per cent of the pulse period. Comparison with the results of Stairs et al. (1999) shows that the leading strong component in Fig. 14 has a very steep spectrum as

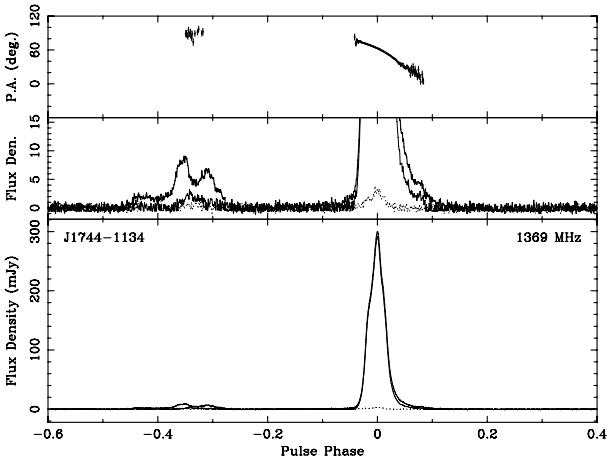

Figure 13. Polarization profiles for PSR J1744−1134 at 1369 MHz. See Fig. 1 for further details.

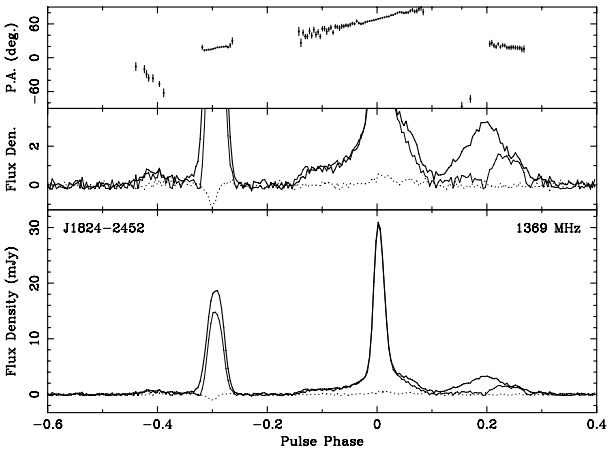

Figure 14. Polarization profiles for PSR J1824−2452 at 1369 MHz. See Fig. 1 for further details.

it is by far the strongest component at 610 MHz. Our results are generally in agreement with those of Ord et al. (2004) but show more detail, including a weak component around phase −0.4. Most of the strongest component in Fig. 14 is 100 per cent linearly polarized. In fact, there is slight overpolarization of the ramp preceding this component. This may result from the difficulty in accurately estimating baselines for this very wide profile or from the existence of polarized unpulsed emission from the pulsar. The first strong component is also very highly polarized. The PA variation across these components appears continuous, but the PA of the extreme leading and trailing components is not continuous with the central part, having the opposite slope.

3.15 PSR J1857+0943 (PSR B1855+09)

Our results, shown in Fig. 15, are in excellent agreement with those of Ord et al. (2004), showing a relatively weakly polarized main pulse and interpulse, both of which have multiple components. Thorsett & Stinebring (1990) observed a weak steep-spectrum component just preceding the main pulse, and we see this component as well (at phase −0.1 in Fig. 15). The PA variation is complex across the main pulse and completely inconsistent with the RVM. There is evidence for an orthogonal mode transition near the highest peak of the interpulse (cf. Xilouris et al. 1998).

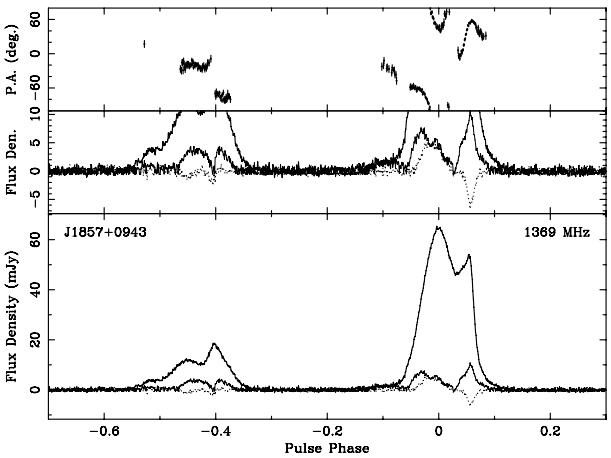

Figure 15. Polarization profiles for PSR J1857+0943 at 1369 MHz. See Fig. 1 for further details.

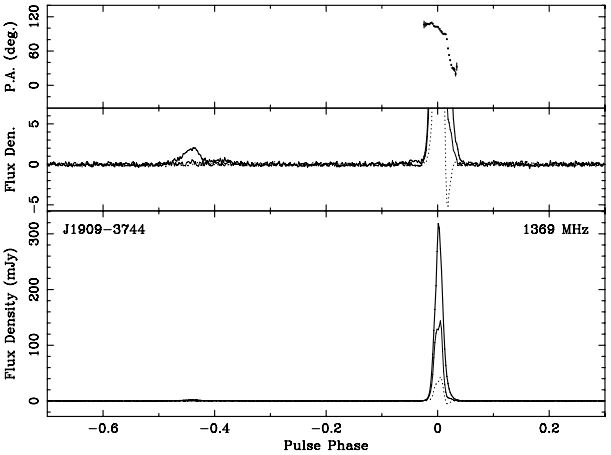

Figure 16. Polarization profiles for PSR J1909−3744 at 1369 MHz. See Fig. 1 for further details.

3.16 PSR J1909−3744

The mean pulse profile for this pulsar has a narrow main pulse and a weak feature preceding the main pulse by about 0.45 in phase. Our observations, shown in Fig. 16, are generally consistent with those of Ord et al. (2004) but show some additional features. The 'interpulse' feature is clearly seen to consist of two components, and there is evidence for a weak shelf of emission immediately preceding the main pulse. The main pulse is moderately polarized and has a PA variation which is almost consistent with the RVM and a very small impact parameter. However, the total PA swing is closer to 90° rather than the expected 180°. This and the coincident sense reversal of circular polarization suggest that the rapid swing is actually a smeared orthogonal transition. The smearing is not instrumental and must be intrinsic to the emitted radiation.

3.17 PSR J1939+2134 (PSR B1937+21)

The mean pulse profile of PSR J1939+2134, the first-discovered MSP (Backer et al. 1982), has a main pulse and a relatively strong interpulse separated by ∼172° or 0.48 in pulse phase. Because of the high DM/P (i.e. the dispersion measure to spin period ratio) of this pulsar, our observations shown in Fig. 17 are significantly affected by DM smearing (see Table 1). As a result, we do not see the secondary maxima at the trailing edges of both pulses seen by Thorsett & Stinebring (1990), Stairs et al. (1999) and Ord et al. (2004), all of whom used coherent dedispersion. However, the high sensitivity of our observations reveals previously undetected pulsed emission preceding both the main pulse and the interpulse by about 0.2 in phase. This emission has a peak flux density about 0.5 per cent of that of the main pulse and appears to have multiple components. At such a low level, one is concerned that otherwise undetected RFI or instrumental problems may be responsible. However, when the data set is split in both frequency and time, the low-level components are visible in all of the partial data sets. Although low-level features have been detected in a number of pulsars in this study, in general they do not have the same relationship to the main pulse emission as is seen for PSR J1939+2134. Furthermore, for PSR J1939+2134, the emission preceding the interpulse has a different profile to that preceding the main pulse. For these reasons, we believe that the low-level emission seen in Fig. 17 is real and is not either an instrumental artefact or due to RFI.

The polarization properties shown in Fig. 17 are generally consistent with previously published polarimetry (Thorsett & Stinebring 1990; Stairs et al. 1999; Ord et al. 2004), although we see more significant left-circular emission, especially in the main pulse. All three of the earlier papers referred to above find evidence for an orthogonal mode transition near the leading edge of the main pulse. However, our data suggest that the jump is closer to 60° and therefore not orthogonal. On the other hand, there is some evidence for a reversal in the sense of circular polarization at the phase of the PA transition. We also see a previously undetected orthogonal transition near the trailing edge of the interpulse. Thorsett & Stinebring (1990) and Stairs et al. (1999) find evidence for an orthogonal jump at low frequencies near the leading edge of the interpulse, but no evidence for jumps at frequencies around 1400 MHz.

3.18 PSR J2124−3358

As Fig. 18 shows, this pulsar has an extremely complicated multicomponent mean pulse profile with emission covering nearly the entire pulse period. The polarization profiles presented here are in good agreement with those presented by Manchester & Han (2004) and Ord et al. (2004) for frequencies around 1400 MHz. The fractional linear polarization changes greatly across the profile with the emission near phase −0.4 being essentially 100 per cent linearly polarized, whereas, on average, the profile is about 18 per cent

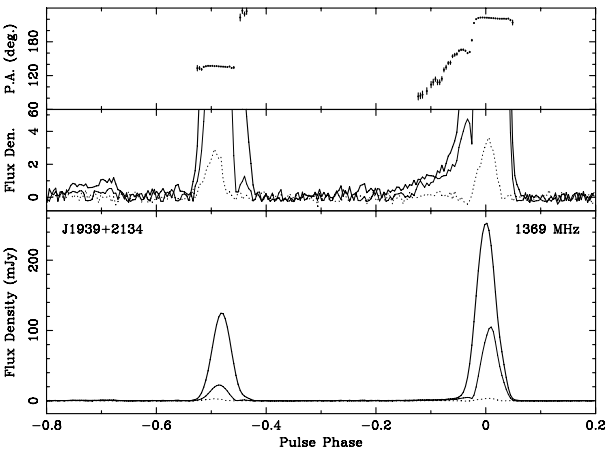

Figure 17. Polarization profiles for PSR J1939+2134 at 1369 MHz. See Fig. 1 for further details.

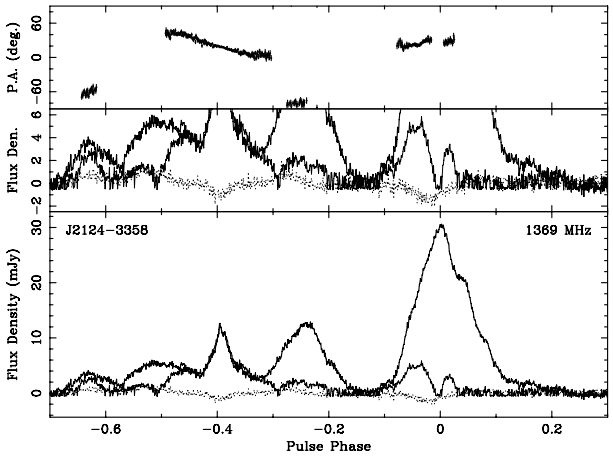

Figure 18. Polarization profiles for PSR J2124−3358 at 1369 MHz. See Fig. 1 for further details.

polarized (Table 2). As discussed by Manchester & Han (2004), the fact that no 'superpolarization' is seen suggests that there is no strong steady emission from the pulsar. We confirm that weak but significant right-circular polarization is present for the components near phase zero and phase −0.4 in Fig. 18. In agreement with previous work, an orthogonal mode transition is seen near phase −0.3. If the PAs for emission between phases of −0.3 and −0.2 and those for the leading portion of the profile (to phase −0.5, see Manchester & Han 2004) are raised by 90°, then the PA variation approximates an RVM variation for an outer line of sight with the magnetic axis aligned at about 25° to the rotation axis. Such a nearly aligned system may explain the fact that we see emission over most if not all of the pulse period.

3.19 PSR J2129−5721

This pulsar has been studied at 659 and 1331 MHz by Manchester & Han (2004) and at 1373 MHz by Ord et al. (2004). The results shown in Fig. 19 are in agreement with these earlier results, but show more detail. All observations detect the post-cursor and a weaker leading shelf of emission, but the present results show that this extends to at least phase −0.2, giving the pulse an overall width of at least 0.4 in phase. The PA mostly decreases through the pulse, but the present results clearly show a PA 'glitch' at the phase of the trailing main-pulse component. The degree of circular polarization is unusually high, especially for the trailing main-pulse component. On average, it is 23 per cent right-circularly polarized, the second highest in Table 2 after PSR J1603−7202.

3.20 PSR J2145−0750

The polarimetry of this relatively strong MSP (mean flux density at 9.3 mJy, third to PSR J0437−4715 and PSR J1939+2134, Table 2) has been studied by a number of groups (Stairs et al. 1999; Manchester & Han 2004; Ord et al. 2004). Our results, presented in Fig. 20, are generally in good agreement with these earlier authors, but show more detail. Both Manchester & Han (2004) and Ord et al. (2004) found a weak bridge of emission between the leading and main pulse components, but we do not see a bridge. The apparent bridge in the earlier results is probably an artefact arising from the 2-bit digitization of the input bandpass employed in these systems. Our results show structure in the leading component with at least two subcomponents. In agreement with earlier work, this

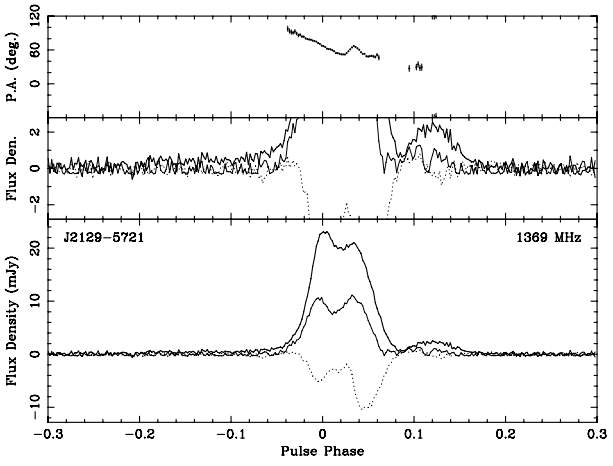

Figure 19. Polarization profiles for PSR J2129−5721 at 1369 MHz. See Fig. 1 for further details.

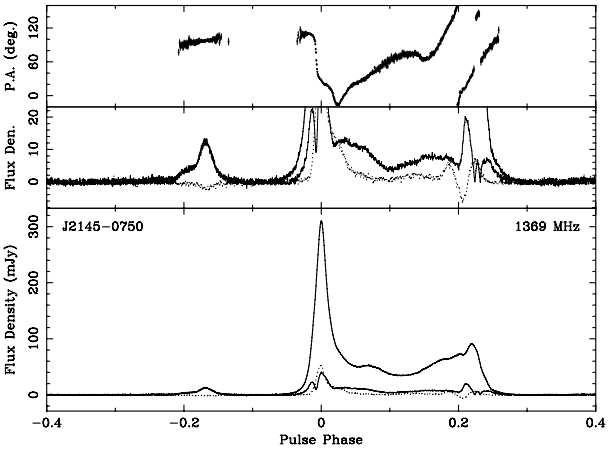

Figure 20. Polarization profiles for PSR J2145−0750 at 1369 MHz. See Fig. 1 for further details.

component is essentially 100 per cent linearly polarized and has an almost constant PA. The PA variation in the rest of the profile is very complex with regions of increasing and decreasing PAs. There are remarkably close orthogonal transitions (up and back) at phases 0.223 and 0.231 with corresponding dips in *L*. There are also sense changes in *V* at phases 0.197 and 0.215, but these do not seem to be associated with the orthogonal mode jumps which are slightly later in phase.

4 ROTATION MEASURES

Many of the PPTA pulsars either did not have published RMs or the published values were insufficiently accurate for summing our data across frequency to form final profiles. As described in Section 2, the variable ionospheric RM was subtracted from the measured values to give an accurate estimate of the interstellar RM for each pulsar. Table 3 gives our estimates of the interstellar RM together with the Galactic coordinates and distance [estimated from the DM using the Cordes & Lazio (2002) model] of the pulsar and previously published RM values. In some cases, the previously published values do not have the ionospheric component removed, but this would generally be smaller than the quoted uncertainty. We also give the mean value of the line-of-sight component of the interstellar magnetic field in microgauss weighted by the local electron density along the path (equation 6). Negative values correspond to fields directed away from the Earth.

In most cases, our RM measurements are close to previous measurements within the uncertainties. However, PSR J1824−2452 (PSR B1821−24) stands out; in this case, it seems likely that the previously published result was incorrect. For several other pulsars, the results differ by more than the combined error. There are several possible reasons for this. Perhaps the most likely is that unknown systematic errors, most probably in calibration, resulted in underestimation of the RM uncertainties. Alternatively, it is possible that in some cases there has been a real change in RM since the earlier measurements. Continuing PPTA observations will help to establish if such variations exist.

5 DISCUSSION AND CONCLUSIONS

We have presented new and improved polarization profiles for the 20 MSPs observed as part of the PPTA project. Because of the frequent and relatively long observations needed by the PPTA project,

Table 3. Interstellar RMs for 20 MSPs.

PSR	Gal. l (°)	Gal. b (°)	Dist. (kpc)	RM (this work) (rad m^{-2})	RM (prev. publ.) (rad m^{-2})	$\langle B_{\|\|} \rangle$ (μG)
J0437−4715	253.39	−41.96	0.16	0.0 ± 0.4	1.5 ± 5[a]	−0.0 ± 0.19
J0613−0200	210.41	−9.30	1.25	9.7 ± 1.1	19 ± 14[b]	0.31 ± 0.03
J0711−6830	279.53	−23.28	0.86	21.6 ± 3.1	67 ± 23[b]	1.45 ± 0.21
J1022+1001	231.79	+51.10	0.56	−0.6 ± 0.5	–	−0.07 ± 0.06
J1024−0719	251.70	+40.52	0.53	−8.2 ± 0.8	–	−1.56 ± 0.15
J1045−4509	280.85	+12.25	0.30	92.0 ± 1.0	82 ± 18[b]	1.95 ± 0.02
J1600−3053	344.09	+16.45	5.00	−15.5 ± 1.0	–	−0.36 ± 0.02
J1603−7202	316.63	−14.50	1.17	27.7 ± 0.8	20.1 ± 5[b]	0.90 ± 0.03
J1643−1224	5.67	+21.22	0.45	−308.1 ± 1.0	−263 ± 15[b]	−6.08 ± 0.02
J1713+0747	28.75	+25.22	1.05	8.4 ± 0.6	–	0.65 ± 0.05
J1730−2304	3.14	+6.02	0.53	−7.2 ± 2.2	–	−0.92 ± 0.28
J1732−5049	340.03	−9.45	1.41	−8.5 ± 6.7	–	−0.18 ± 0.15
J1744−1134	14.79	+9.18	0.42	−1.6 ± 0.7	–	−0.63 ± 0.27
J1824−2452	7.80	−5.58	4.90	77.8 ± 0.6	1 ± 12[c]	0.80 ± 0.01
J1857+0943	42.29	+3.06	0.91	16.4 ± 3.5	53 ± 9[d]	1.52 ± 0.32
J1909−3744	359.73	−19.60	1.27	−6.6 ± 0.8	–	−0.78 ± 0.09
J1939+2134	57.51	−0.29	8.33	6.7 ± 0.6	−10 ± 9[c]	0.12 ± 0.01
J2124−3358	10.93	−45.44	0.32	−5.0 ± 0.9	1.2 ± 1[b]	−1.34 ± 0.24
J2129−5721	338.01	−43.57	0.53	23.5 ± 0.8	37.3 ± 2[b]	0.91 ± 0.03
J2145−0750	47.78	−42.08	0.62	−1.3 ± 0.7	12 ± 8[b]	−0.18 ± 0.1

[a]Navarro et al. (1997); [b]Manchester & Han (2004); [c]Rand & Lyne (1994); [d]Han et al. (2006).

our polarization profiles generally have very high S/N compared to earlier results. Also, we have employed improved signal processing procedures, including corrections for feed cross-coupling and ionospheric Faraday rotation. As a result, we have not only defined the polarization properties more accurately, but also revealed previously unknown profile features in many of the pulsars.

In a number of cases, the newly detected profile features greatly extend the range of pulse phase over which emission is detected. For example, in PSR J1045−4509, the detection of a low-level leading component and bridge emission joining it to the main pulse has increased the overall observed width of the pulsed emission by nearly a factor of 3, from about 0.25 to about 0.7 in phase. PSR J1939+2134 (PSR B1937+21) is an interesting case in which the newly detected emission changes the pulse profile from having just a main pulse and interpulse separated by close to 0.5 in phase and both relatively narrow, to a wide profile covering about 80 per cent of the pulse period. In some ways, the situation is similar to that of the Crab pulsar, where pulse components with high linear polarization are detected at phases very different to those of the main pulse and interpulse (Moffett & Hankins 1996, 1999). These pulse components are only seen at high radio frequencies, but the Crab pulsar also has a highly polarized precursor pulse which is only seen at low radio frequencies (Manchester 1971; Moffett & Hankins 1996). Some, but not all, of the outlying components detected in this study are highly linearly polarized, but those in PSR J1939+2134 are not.

Table 2 gives the overall pulse width, that is, the total longitude range over which significant pulsed emission is seen, for each of the PPTA pulsars. The distribution of these widths is plotted in Fig. 21. Only seven of the 20 pulsars have emission spanning less than half of the period and five have emission over more than three quarters of the period. Only in a few of the pulsars does the pulse profile have the form of a main pulse and interpulse separated by close to half the period. Even when there are strong pulse components that can be labelled in this way, there is generally emission at other pulse phases as well.

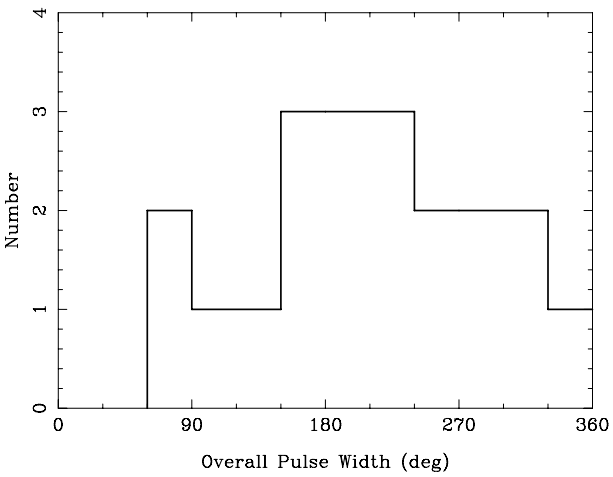

Figure 21. Histogram of overall pulse widths for the 20 PPTA pulsars.

Most normal (non-millisecond) pulsars have mean pulse profiles that can be described within the core–cone framework with one to five clearly identifiable pulse components or peaks within a relatively narrow longitude range, typically about 20°. Although the relative amplitude of the various components varies widely, leading to the notion of partial cones (Lyne & Manchester 1988), there often appears to be a symmetry about a central phase, leading to the idea of nested cones (e.g. Rankin 1990; Gupta & Gangadhara 2003). However, observations with high S/N often show a more complex profile structure with multiple components (e.g. PSR B0740−28 in Kramer 1994) which are not easily accommodated in the nested-cone model. This and the wide variation of component amplitudes led to the idea of 'patchy' emission beams (Lyne & Manchester 1988; Han & Manchester 2001). Pulsars with interpulses and/or wide profiles form another group of multiple-component pulsars. Only a few normal pulsars have these features,

with less than 2 per cent showing interpulse emission (Weltevrede & Johnston 2008) and most of this 2 per cent have short periods and high spin-down luminosities. Many have the main pulse and interpulse separated by close to 180°, but some have smaller spacings and/or bridges of emission between the two components. Good examples are the Crab pulsars as discussed above, PSR B0950+08 and PSR B1929+10 (Hankins & Fowler 1986). Some interpulse pulsars also have weaker pulse components, often highly linearly polarized, separated from the main pulse and interpulse and usually termed 'precursors' or 'post-cursors'. Examples are the Crab pulsars again, PSR B0823+26 (Hankins & Fowler 1986; Rankin & Rathnasree 1995) and PSR B1822−09 (Manchester, Hamilton & McCulloch 1980; Johnston et al. 2007).

As mentioned above, wide profiles and interpulses are much more common in MSPs, with more than 60 per cent of the present sample showing these features. PSR J1045−4509 (Fig. 6) is a good example of a nominal interpulse joined to the main pulse by a bridge of emission. Highly polarized precursors and post-cursors are observed in PSR J1024−0719 (Fig. 5), PSR J1603−7202 (Fig. 8), PSR J1713+0747 (Fig. 10) and PSR J1730−2304 (Fig. 11). Multiple components are ubiquitous in MSPs. Some components are obvious as clearly resolved peaks in the pulse profile, but others are just points of inflection in the profile and probably some are not obvious in the profile at all. Table 2 gives an estimate of the minimum number of identifiable components in the PPTA MSPs based on peaks or points of inflection in the pulse profiles.

In most cases, the observed PA variations across these wide profiles are incredibly complex, even after allowance for orthogonal mode transitions, and are not even approximately described by the RVM. Exceptions are PSR J1024−0719, PSR J1600−3053 and PSR J1732−5049, which have relatively flat PA profiles, and PSR J1022+1001, PSR J1744−1134 and PSR J2124−3358, which have reasonably smooth PA variations that are consistent with the RVM. Except for PSR J1022+1001, RVM fits to these PA variations imply large impact parameters and/or nearly aligned magnetic and rotational axes. For PSR J2124−3358, a nearly aligned model may well be the correct interpretation since it has emission across essentially the whole period, but in other cases it is not so clear.

For most of the pulsars observed, the PA variations are complex with disconnected PA segments, often with opposite slopes in neighbouring regions (e.g. PSR J0613−0200, Fig. 2; PSR J1603−7202, Fig. 8; PSR J1730−2304, Fig. 11; PSR J2145−0750, Fig. 20) and non-orthogonal PA jumps (e.g. PSR J0437−4715, Fig. 1; PSR J0711−6830, Fig. 3; PSR 1713+0747, Fig. 10). Within a single component, the PA variation is usually continuous and monotonic (orthogonal jumps excepted). These results suggest that overlapping components may originate in different locations within the magnetosphere. Supporting evidence for quasi-independent emission regions comes from phase-resolved spectral index plots which show different spectral indices for different components (e.g. Manchester & Han 2004). Dyks, Rudak & Demorest (2010a) have also suggested the idea of independent emission from different parts of the pulsar magnetosphere, in their case, from thin plasma streams emitting coherent curvature radiation. In this model, the symmetry axis for PA variations is not the magnetic axis (as in the dipole polar-cap model) but the plasma stream direction. This could certainly account for the non-RVM PA variations we observe. However, we do not find evidence for the common occurrence of the double features they identify with the basic curvature radiation beam.

The very wide MSP profiles we observe (Fig. 21) imply large emission heights in the simple polar-cap model. In fact, for a pulsar period of 4 ms and an overall pulse width of 200° (about the median values for our sample), equation (2) implies $r/R_{\rm LC} \gtrsim 1.3$. One could invoke small inclination angles, but it is more likely that the equation is simply not applicable. Similarly, the standard methods for estimating emission heights cannot be applied to MSPs. They do not exhibit radius–frequency mapping of component separations, and hence that method (Cordes 1978) cannot be used. Likewise, the method of Blaskiewicz et al. (1991), which relies on identifying a relativistic aberration/retardation shift between the pulse profile and the PA variations, cannot be applied because of the general lack of symmetry about a central longitude for one or both properties. For example, PSR J0437−4715 and PSR J2145−0750 both have reasonably symmetric pulse profiles, but in both cases it is impossible to determine any symmetry centre for the PA variations. Relativistic methods which rely on a height difference between core and conal components (Gupta & Gangadhara 2003; Dyks, Rudak & Harding 2004) also cannot easily be applied to MSPs since it is generally impossible to uniquely identify components as either core or cone.

Based on associations with gamma-ray detections, Manchester (2005) and Ravi, Manchester & Hobbs (2010) argued that radio beams from young and MSPs are emitted from the outer magnetosphere and that caustic effects are important in defining the observed pulse profile. By analogy with gamma-ray pulse profiles (e.g. Dyks & Rudak 2003; Watters et al. 2009), such effects may account for the broad frequency-independent pulse profiles observed in MSPs, including interpulses and connecting bridges. The results presented in this paper support this idea. The observed pulse profiles are too wide and too complex to be simply accounted for as emission tangential to the open field lines at low altitudes in the pulsar magnetosphere. Observed PA variations are also generally inconsistent with this interpretation. For example, the extended low-level emission observed for PSR J1939+2134 (Fig. 17) shows that main pulse and interpulse in this pulsar are not simple polar beams from opposite magnetic poles as was originally thought. In this context, it is important to note that, for both the Crab pulsar and PSR J1939+2134, giant radio pulses occur at phases closely related to the phase of the high-energy emission and to the main radio peaks (Cusumano et al. 2003; Abdo et al. 2010; Molkov et al. 2010) also supporting the idea of the radio emission originating in the outer magnetosphere.

Dyks et al. (2010b) discussed the caustic deformation of radio pulse profiles by aberration and retardation, albeit to a more modest degree than that proposed above. Trailing sides of profiles are compressed in width and enhanced in amplitude, whereas leading parts are spread out and reduced in amplitude. They apply these ideas to the main pulse of the MSP PSR J1012+5307, which has a strong trailing component and a weaker, more extended leading part, and model the observed profile with a patchy underlying emission and a small relativistic deformation, with the emission originating between the stellar surface and twice that radius. Of the pulsars we observed, only PSR J1022+1001 and maybe PSR J1600−3035 have similar profiles with a relatively strong and narrow trailing component. It is clear that these ideas are not generally applicable to MSPs.

Johnston & Weisberg (2006) suggested that emission from many young pulsars arises from the outermost open field lines at relatively high altitudes, between 5 and 15 per cent of the light cylinder radius. We are proposing that for MSPs (and some young pulsars as well), the emission zone extends much higher, up to or even beyond the null-charge surface, with caustic deformations a dominant influence on the profile morphology. To account for the multiple components and complex PA variations observed in MSPs, much structure is

required in the underlying emission. This could originate from isolated plasma streams as suggested by Dyks et al. (2010a) with the observed PA determined by the projection of the stream axis or by the local magnetic field direction. In the outer magnetosphere, such currents will significantly deform the basic dipolar field, leading to the observed small-scale PA variations and discontinuities. It is worth noting though that the observed complex profile and PA variations are extremely stable over time-scales of decades [compare the PSR J0437−4715 profiles in Navarro et al. (1997) and in Fig. 1]. Observations of nulling and mode changing in normal pulsars (e.g. Wang, Manchester & Johnston 2007; Lyne et al. 2010) show that magnetospheric currents can vary on short time-scales, but to date there is little evidence that such phenomena exist in MSPs. Even in normal pulsars, the properties of a given mode seem quite stable. Inwardly directed emission beams from charges flowing towards the neutron star (Gil et al. 1994; Dyks et al. 2005) provide another possible explanation for the multiple and overlapping components of MSP pulse profiles.

Despite the generally more complex pulse profiles of MSPs compared to normal pulsars, there are many similarities in the emission characteristics. Fractional linear polarizations are often very high for both classes of pulsar, orthogonal mode transitions are ubiquitous in both classes and circular polarization is often seen, but is almost always weaker than the linear polarization. Truly orthogonal polarization transitions (both circular and linear changing sign) do seem more common in MSPs with at least five clear examples (in PSR J0437−4715, PSR J1600−3053, two in PSR J1643−1224 and PSR J1713+0747) among the 20 PPTA pulsars presented here. Overall though, the similarities in polarization behaviour outweigh the differences, strongly suggesting that the basic radio emission mechanism is the same for both normal pulsars and MSPs.

We derive RMs for all 20 pulsars, eight of which have no previously published RMs. For those with previously published RMs, our measurements have smaller estimated uncertainties and we believe they are more accurate than the previous values. For three pulsars (PSR J1824−2452, PSR J1939+2134 and PSR J2145−0750), our measurements differ significantly, indicating systematic errors, most probably in the earlier measurements. RMs and implied mean values of the line-of-sight component of the interstellar magnetic field are small for high-latitude and more distant pulsars in accord with earlier results (e.g. Han et al. 2006). Most measured values are less than or about 1 μG, but that for PSR J1643−1224 at 6 μG is an exception. The estimated distance for this pulsar is only about 0.5 kpc, and the path to it traverses the North Polar Spur (Wolleben 2007). The large mean field strength almost certainly results from compressed interstellar fields in the shell(s) which form this prominent feature of the Galactic radio background.

ACKNOWLEDGMENTS

The PPTA project is a collaboration between a number of groups both in Australia and in other countries established with the support of RNM's Australian Research Council Federation Fellowship (#FF0348478). GH is the recipient of an Australian Research Council QEII Fellowship (#DP0878388). WMY is supported by NSFC project 10673021, the Knowledge Innovation Programme of the Chinese Academy of Sciences, grant no. KJCX2-YW-T09 and National Basic Research Programme of China (973 Programme 2009CB824800). We thank members of the PPTA collaboration who assisted with the observations reported in this paper. We thank Andrew Gray and Ken Tapping for making the Penticton ionospheric modelling program available to us. The Parkes radio telescope is part of the Australia Telescope, which is funded by the Commonwealth of Australia for operation as a National Facility managed by the Commonwealth Scientific and Industrial Research Organisation.

REFERENCES

Abdo A. A. et al., 2010, ApJ, 708, 1254
Backer D. C., 1976, ApJ, 209, 895
Backer D. C., Rankin J. M., 1980, ApJS, 42, 143
Backer D. C., Kulkarni S. R., Heiles C., Davis M. M., Goss W. M., 1982, Nat, 300, 615
Blaskiewicz M., Cordes J. M., Wasserman I., 1991, ApJ, 370, 643
Cordes J. M., 1978, ApJ, 222, 1006
Cordes J. M., Lazio T. J. W., 2002, preprint (astro-ph/0207156)
Cusumano G. et al., 2003, A&A, 410, L9
Dyks J., Rudak B., 2003, ApJ, 598, 1201
Dyks J., Rudak B., Harding A. K., 2004, ApJ, 607, 939
Dyks J., Frąckowiak M., Słowikowska A., Rudak B., Zhang B., 2005, ApJ, 633, 1101
Dyks J., Rudak B., Rankin J. M., 2007, A&A, 465, 981
Dyks J., Rudak B., Demorest P., 2010a, MNRAS, 401, 1781
Dyks J., Wright G. A. E., Demorest P., 2010b, MNRAS, 405, 509
Gil J. A. et al., 1994, A&A, 282, 45
Gupta Y., Gangadhara R. T., 2003, ApJ, 584, 418
Han J. L., Manchester R. N., 2001, MNRAS, 320, L35
Han J. L., Manchester R. N., Lyne A. G., Qiao G. J., van Straten W., 2006, ApJ, 642, 868
Han J. L., Demorest P. B., van Straten W., Lyne A. G., 2009, ApJS, 181, 557
Hankins T. H., Fowler L. A., 1986, ApJ, 304, 256
Hobbs G. B., Edwards R. T., Manchester R. N., 2006, MNRAS, 369, 655
Hobbs G. B. et al., 2009, PASA, 26, 103
Hotan A. W., van Straten W., Manchester R. N., 2004, PASA, 21, 302
Johnston S., Weisberg J. M., 2006, MNRAS, 368, 1856
Johnston S. et al., 1993, Nat, 361, 613
Johnston S., Kramer M., Karastergiou A., Hobbs G., Ord S., Wallman J., 2007, MNRAS, 381, 1625
Komesaroff M. M., 1970, Nat, 225, 612
Kramer M., 1994, A&AS, 107, 527
Kramer M., Xilouris K. M., Lorimer D. R., Doroshenko O., Jessner A., Wielebinski R., Wolszczan A., Camilo F., 1998, ApJ, 501, 270
Kramer M., Xilouris K. M., Camilo F., Nice D., Lange C., Backer D. C., Doroshenko O., 1999, ApJ, 520, 324
Lorimer D. R., Kramer M., 2005, Handbook of Pulsar Astronomy. Cambridge Univ. Press, Cambridge
Lyne A. G., Manchester R. N., 1988, MNRAS, 234, 477
Lyne A. G., Smith F. G., 1968, Nat, 218, 124
Lyne A. G., Brinklow A., Middleditch J., Kulkarni S. R., Backer D. C., Clifton T. R., 1987, Nat, 328, 399
Lyne A., Hobbs G., Kramer M., Stairs I., Stappers B., 2010, Sci, 329, 408
McKinnon M., Stinebring D., 1998, ApJ, 502, 883
Manchester R. N., 1971, ApJ, 163, L61
Manchester R. N., 1974, ApJ, 188, 637
Manchester R. N., 1995, JA&A, 16, 107
Manchester R. N., 2005, Ap&SS, 297, 101
Manchester R. N., 2008, in Bassa C., Wang Z., Cumming A., Kaspi V. M., eds, AIP Conf. Proc. Vol. 983, 40 Years of Pulsars: Millisecond Pulsars, Magnetars and More. Am. Inst. Phys., New York, p. 584
Manchester R. N., Han J. L., 2004, ApJ, 609, 354
Manchester R. N., Johnston S., 1995, ApJ, 441, L65
Manchester R. N., Taylor J. H., Huguenin G. R., 1975, ApJ, 196, 83
Manchester R. N., Hamilton P. A., McCulloch P. M., 1980, MNRAS, 192, 153
Manchester R. N. et al., 2010, ApJ, 710, 1694
Moffett D. A., Hankins T. H., 1996, ApJ, 468, 779
Moffett D. A., Hankins T. H., 1999, ApJ, 522, 1046
Molkov S., Jourdain E., Roques J. P., 2010, ApJ, 708, 403

Navarro J., Manchester R. N., Sandhu J. S., Kulkarni S. R., Bailes M., 1997, ApJ, 486, 1019
Noutsos A., Johnston S., Kramer M., Karastergiou A., 2008, MNRAS, 386, 1881
Ord S. M., van Straten W., Hotan A. W., Bailes M., 2004, MNRAS, 352, 804
Petrova S. A., 2001, A&A, 378, 883
Radhakrishnan V., Cooke D. J., 1969, Astrophys. Lett., 3, 225
Rand R. J., Lyne A. G., 1994, MNRAS, 268, 497
Rankin J. M., 1983, ApJ, 274, 333
Rankin J. M., 1990, ApJ, 352, 247
Rankin J. M., 1993, ApJ, 405, 285
Rankin J. M., Rathnasree N., 1995, JA&A, 16, 327
Ravi V., Manchester R. N., Hobbs G., 2010, ApJ, 716, L85
Stairs I. H., Thorsett S. E., Camilo F., 1999, ApJS, 123, 627
Staveley-Smith L. et al., 1996, PASA, 13, 243
Stinebring D. R., Cordes J. M., Rankin J. M., Weisberg J. M., Boriakoff V., 1984, ApJS, 55, 247
Thorsett S. E., Stinebring D. R., 1990, ApJ, 361, 644
van Straten W., 2004, ApJS, 152, 129
van Straten W., Manchester R. N., Johnston S., Reynolds J. E., 2010, PASA, 27, 104
Wang N., Manchester R. N., Johnston S., 2007, MNRAS, 377, 1383
Watters K. P., Romani R. W., Weltevrede P., Johnston S., 2009, ApJ, 695, 1289
Weltevrede P., Johnston S., 2008, MNRAS, 387, 1755
Wolleben M., 2007, ApJ, 664, 349
Xilouris K. M., Kramer M., Jessner A., von Hoensbroech A., Lorimer D., Wielebinski R., Wolszczan A., Camilo F., 1998, ApJ, 501, 286

This paper has been typeset from a TEX/LATEX file prepared by the author.